Available online at www.sciencedirect.com
ScienceDirect
C. R. Physique 10 (2009) 148–158
COMPTES RENDUS PHYSIQUE

Laser acceleration of particles in plasmas / Accélération laser de particules dans les plasmas

Physics of colliding laser pulses in underdense plasmas

Jérôme Faure [a,*], Clément Rechatin [a], Ahmed Ben-Ismail [a,b], Jaeku Lim [a], Xavier Davoine [c], Erik Lefebvre [c], Victor Malka [a]

[a] *Laboratoire d'optique appliquée, ENSTA, CNRS, École polytechnique, UMR 7639, 91761 Palaiseau, France*
[b] *Laboratoire Leprince-Ringuet, École polytechnique, CNRS-IN2P3, UMR 7638, 91128 Palaiseau, France*
[c] *CEA, DAM, DIF, Bruyères-le-Châtel, 91297 Arpajon cedex, France*

Available online 25 April 2009

Abstract

We report on recent experimental results on electron acceleration using two counter-propagating ultrashort and ultraintense laser pulses. At the collision, the two pulses drive a standing wave which is able to pre-accelerate plasma electrons which can then be trapped in the plasma wave. Optical diagnostics of the collision reveal signatures of this standing wave. Electron acceleration results in this regime are reviewed: the use of colliding pulses enables the generation of stable, tunable and high quality electron beams at the 100–200 MeV level. Detailed comparisons with 3D Particle in Cell (PIC) simulations give deeper insight on the role of the nonlinear propagation of the pump pulse on the performance of the accelerator. This deeper understanding has allowed us to optimize the beam charge of the accelerator at high energy. ***To cite this article: J. Faure et al., C. R. Physique 10 (2009).***

Résumé

Physique de la collision d'impulsions laser intenses dans les plasmas sous-denses. Des résultats récents sur l'accélération d'électrons par collision d'impulsions laser intenses et contre propagatives sont présentés. À la collision, l'interférence des deux impulsions conduit à la génération d'une onde stationnaire qui pré-accélère les électrons du plasma qui, par la suite pourront être piégés dans l'onde de sillage. Les diagnostics optiques de la région de collision mettent en évidence des signatures de la présence de cette onde stationnaire. Une revue des résultats d'accélération d'électrons est ensuite présentée : l'utilisation de la technique d'injection par collision d'impulsions permet la production de faisceaux d'électrons stables, réglables et de haute qualité dans la gamme d'énergie 100–200 MeV. Les simulations PIC en trois dimensions révèlent le rôle important de la dynamique nonlinéaire de la propagation du faisceau pompe et son impact sur les performances de l'accélérateur. La prise en compte de ces effets nous a permis d'optimiser la charge à haute énergie du faisceau d'électrons. ***Pour citer cet article : J. Faure et al., C. R. Physique 10 (2009).***

Keywords: Laser–plasma interaction; Electron acceleration; Colliding pulses

Mots-clés : Interaction laser–plasma ; Accélération d'électrons ; Collision d'impulsions laser

* Corresponding author.
E-mail address: jerome.faure@ensta.fr (J. Faure).

1631-0705/$ – see front matter
doi:10.1016/j.crhy.2009.03.006

1. Introduction

In laser–plasma-based accelerators [1], an intense laser pulse drives a large electric field (the wakefield) which accelerates particles to high energies in distances much shorter than in conventional accelerators. These high acceleration gradients, of a few hundreds of gigavolts per meter, hold the promise of compact high-energy particle accelerators. Such electric fields have been measured and used to accelerate electrons in many laboratories, but the controlled injection of electrons in these wakefields is still an open issue. When the plasma wave is linear, its shape is quasi-sinusoidal and plasma electrons, which have no initial velocity, are not trapped by the wakefield and consequently, not accelerated. When the plasma wave becomes severely nonlinear, transverse wave breaking effects [2] can result in the self-trapping of electrons in the so-called "bubble" (or blow out) regime [3,4]. This phenomenon has been observed in 2004 in [5–7] where quasi-monoenergetic electron beams at the 100 MeV level were obtained. At the time of those first experiments, stability and control of the beam parameters were not addressed. Recently, experiments have shown that controlling the propagation of the laser pulse in a guiding structure seems to improve the electron beam stability [8,9]. Other experiments have also reported on increased stability even though nonlinearities were still dominating the physics of injection [10,11].

Nevertheless, in this scheme, self-injection and acceleration depend on the precise evolution of the laser pulse which makes it difficult to achieve fine control over the electron beam. The precise control of electron injection would permit good tailoring of the electron beam parameters, and would be most useful for applications. Electron injection can be controlled in several ways: (i) by injecting an external electron beam from a conventional accelerator [12,13]; (ii) by triggering injection in a density ramp [14,15]; (iii) by taking advantage of ionization mechanisms [16]; (iv) by using additional laser pulses [17–19]. The idea of using an additional laser pulse for injecting electrons was first proposed by Umstadter et al. [17]. It was further developed by Esarey et al. [18], who proposed a scheme based on counter-propagating laser pulses. In its simplest form, the scheme uses two counter-propagating ultra-short laser pulses with the same central wavelength and polarization. The first laser pulse, the "pump" pulse, creates a wakefield, whereas the second laser, the "injection" pulse, is only used for injecting electrons. The laser pulses collide in the plasma and their interference creates a laser beatwave pattern which can pre-accelerate plasma background electrons. If the laser intensities are high enough, this pre-acceleration permits the injection and trapping of electrons in the wakefield and further acceleration to relativistic energies. Analytical work [20] and simulations [20,21] have shown that this two-stage acceleration mechanism can lead to the production of high quality electron bunches, with narrow energy spread, small divergence and ultra-short duration, even when using relatively modest lasers (e.g. with normalized vector potential $a_0 = 1$ for the pump pulse, and $a_1 = 0.3$ for the injection pulse). Experiments have shown that colliding pulse injection leads to the generation of high quality stable electrons beams and that it gives the possibility of tuning the beam parameters [22,23].

This article presents a review of experimental results on colliding pulse injection. In Section 2, we will first review some theoretical aspects of electron injection by colliding pulses; we will present the experimental set-up in Section 3. Section 4 will focus on optical measurements of the light emitted at the collision and propose an interpretation of the data. Section 5 will present electron beam results. We show that detailed understanding of the injection process has allowed us to optimize the beam charge at high energy.

2. Review of the theory

A theoretical description of electron injection by colliding laser pulses was first proposed by Esarey et al. in Ref. [18]. We will briefly review the principles of their fluid model. Here, for the sake of simplicity, we will restrict ourselves to a 1D description.

First, the pump laser, with normalized vector potential $a_0 = eA_0/mc$, excites a plasma wave – or wakefield – with normalized potential $\phi_0 = e\Phi_0/mc^2$ (e and m are respectively the charge and mass of the electron, c is the speed of light). Let us now consider electron dynamics in the plasma wave potential ϕ_0 (behind the laser pulse). It is governed by the following Hamiltonian:

$$H = \left(1 + u_z^2\right)^{1/2} - \beta_p u_z - \phi_0 \tag{1}$$

where $u_z = p_z/mc$ is the normalized longitudinal momentum of the electron, and $\beta_p = v_p/c$ is the normalized phase velocity of the wakefield. Before the arrival of the laser pulse, the plasma background electrons are initially at rest.

In the absence of wavebreaking and self-trapping these electrons are not trapped in the plasma wave. They simply oscillate back and forth in the plasma wave potential along an untrapped orbit. The plasma electrons follow the so-called "fluid orbits" and their momenta oscillate between $u_{z,min}^{fluid}$ and $u_{z,max}^{fluid}$

$$u_{z,max,min}^{fluid} = \beta_p \gamma_p^2 \left(1 + \phi_0^{min,max}\right) - \gamma_p \sqrt{\gamma_p^2 \left(1 + \phi_0^{min,max}\right)^2 - 1} \tag{2}$$

where $\phi_0^{min,max}$ represent the minima (maxima) of the potential; $\gamma_p = (1 - \beta_p^2)^{-1/2} = \omega_0/\omega_p$ and ω_0, ω_p are respectively the laser and plasma frequencies. In order to be accelerated in the wakefield, electrons need to move along trapped orbits. The separatrix is the orbit which lies at the separation between trapped and untrapped orbits. When electrons move along the separatrix, their momenta oscillate between $u_{z,min}^{sep}$ and $u_{z,max}^{sep}$

$$u_{z,max,min}^{sep} = \beta_p \gamma_p (1 + \gamma_p \Delta\phi) \pm \gamma_p \sqrt{(1 + \gamma_p \Delta\phi)^2 - 1} \tag{3}$$

where $\Delta\phi = \phi_0^{max} - \phi_0^{min}$.

Thus, one needs to find a mechanism for pushing plasma background electrons, which follow the fluid trajectories, into trapped trajectories. The interference of two laser pulses generates a beatwave which is able to heat electrons and provides such a mechanism. The laser pulses are represented by their normalized vector potential $\mathbf{a_{0,1}}$, where subscripts (0, 1) represent respectively the pump pulse and the injection pulse. Assuming that the lasers are counter-propagating along the z direction, one can write the normalized vector potential as

$$\mathbf{a_{0,1}} = a_{0,1}(\zeta_{0,1}) \left[\cos(k_{0,1}\zeta_{0,1})\mathbf{e_x} + \sigma \sin(k_{0,1}\zeta_{0,1})\mathbf{e_y}\right] \tag{4}$$

where $\sigma = 0$ for linear polarization and $\sigma = 1$ for circular polarization, $k_0 = -k_1$ are the wave vectors and $\zeta_{0,1} = z \pm v_p t$. Although in general the two waves can have different frequencies, to describe the experiments reported here, we have assumed that the two laser pulses have the same frequency ω_0.

When the two pulses overlap, they can interfere and the resulting squared electro-magnetic field can be written as $\mathbf{a}^2 = \mathbf{a_0^2} + \mathbf{a_1^2} + 2\mathbf{a_0} \cdot \mathbf{a_1}$. The last term is the beatwave term and it cancels out for crossed polarizations. In the case where the two polarizations are parallel, it generates a standing wave (i.e. the beatwave has zero phase velocity) with a spatial scale of $\lambda_0/2$. The ponderomotive force in the beatwave is very large (because $F_{beat} = 2k_0 a_0 a_1$) and it can pre-accelerate the plasma electrons. Neglecting the plasma potential, electron trajectories in the beatwave are governed by the Hamiltonian

$$H_b = \sqrt{1 + u_z^2 + \mathbf{a}^2} \tag{5}$$

In order to obtain an analytical estimate, we will assume circular polarization for the pump and injection beam, so that $\mathbf{a}^2 = a_0^2 + a_1^2 + 2a_0 a_1 \cos(2k_0 z)$. The separatrix in this beatwave pattern is then given by

$$u_z^{beat} = \pm\sqrt{2a_0 a_1 (1 - \cos 2k_0 z)} \tag{6}$$

so that on the beatwave separatrix, electrons oscillate between $u_{z,min}^{beat}$ and $u_{z,max}^{beat}$

$$u_{z,max,min}^{beat} = \pm 2\sqrt{a_0 a_1} \tag{7}$$

In Ref. [18], the authors define an approximate threshold for injection into the wakefield by applying a phase space separatrix overlap condition. Specifically, island overlap requires the following conditions: $u_{z,max}^{beat} > u_{z,min}^{sep}$ and $u_{z,min}^{beat} < u_{z,min}^{fluid}$.

Using this criterion, we find that the injection threshold can be reached with $a_0 \simeq 0.7$ and $a_1 \simeq 0.2$ (for this estimation, we have used pulse durations $\tau = 30$ fs and plasma density $n_e = 5 \times 10^{18}$ cm^{-3} in order to calculate the plasma wave amplitude ϕ_0).

When the pulse polarizations are linear, the Hamiltonian in Eq. (5) is time dependent and it is no longer integrable. It has been shown that in this case, electron motion is stochastic [24–26] and the simple calculations presented above do not hold. In fact, stochastic heating turns out to be an efficient mechanism for heating and subsequently injecting electrons. In spite of stochastic heating, electrons are still mainly confined to the micro-buckets at $\lambda_0/2$ in the standing

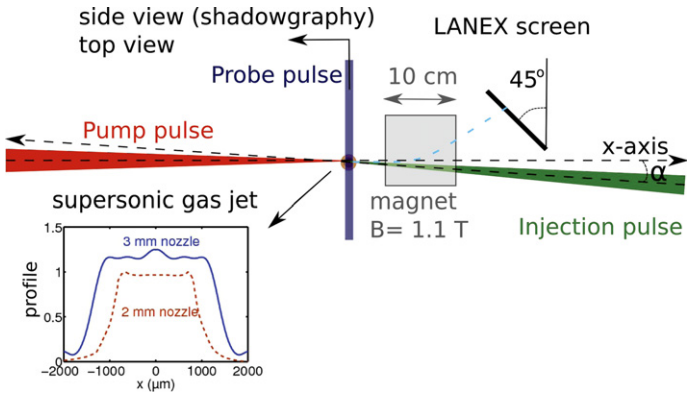

Fig. 1. Experimental setup of the experiment and gas jet density profiles measured by interferometry. In the first experiment, the laser pulses were collinear $\alpha = 0$, in the second experiment, $\alpha = 4°$.

wave. Thus, at the collision, the electron density is strongly modulated at $\lambda_0/2$ which gives rise to a plasma beatwave potential ϕ_b. In the linear limit, $a_0^2 \ll 1$ and $\phi_b \ll 1$, the fluid equation for ϕ_b is [18]

$$\left(\frac{\partial^2}{\partial t^2} + \omega_p^2\right)\phi_b = \omega_p^2 \langle \mathbf{a_0}.\mathbf{a_1} \rangle \tag{8}$$

Assuming that the laser pulses have flat top profiles and that they start to collide at $t = 0$, an analytical solution of Eq. (8) is given by [27]

$$\phi_b = \frac{a_0 a_1}{4}\left[1 - \cos(\omega_p t)\right]\cos(2k_0 x) \tag{9}$$

The spatial scale of ϕ_b is $\lambda_0/2$ and it oscillates at ω_p. It has been discussed [18,20] that this potential plays little role in the heating of plasma electrons. However, note that this potential gives rise to an electron density perturbation δn_b which can be quite large since $\delta n_b/n_0 \simeq (2k_0/k_p)^2\phi_b$ (strictly speaking the linear regime imposes that $\delta n_b/n_0 \ll 1$). Thus, during the collision of the laser pulses, one expects to witness a strong density modulation at $\lambda_0/2$. This modulation is a signature of the standing wave which is used for heating plasma electrons and injecting them in plasma waves.

3. Experimental setup

In this article, we will present the results of two experimental campaigns which were performed at the Laboratoire d'optique appliquée. Experiments were conducted using the "Salle Jaune", titanium doped sapphire laser system which delivers two ultrashort 30 fs linearly polarized pulses. Typical intensities lead to the following range of normalized vector potential for the pump pulse: $a_0 = 1.3$–1.5, and for the injection pulse: $a_1 = 0.4$. In the two experiments, the physical parameters were relatively close to each other but there were two main differences: (i) in the first experiment, a 2 mm supersonic gas jet was used, whereas in the second experiment, the gas jet length was 3 mm; (ii) in the first experiment, the two beams were counterpropagating with a perfectly collinear geometry, whereas in the second experiment, there was a small angle ($\alpha = 4°$) between the counter-propagating laser pulses. A schematic of the experimental setup is shown in Fig. 1. The gas jet profiles were characterized by interferometry and are also shown in Fig. 1. The pump pulse propagates along the x-axis and the injection pulse is counter-propagating with angle α (the point at $x = 0$ represents the center of the gas jet). Having non collinear pulses ($\alpha \neq 0$, as in the second experiment) offers several advantages: (i) it minimizes laser feedback which could potentially damage the laser system (we measured less than 1 mJ of laser feedback); (ii) the electron beam can be used and diagnosed more easily because there are no optics in its path. In addition, because the angle is small, the spatial overlap between the two pulses still occurs over a relatively long distance: $L_{overlap} = 2(w_0 + w_1)/\tan\alpha$, where w_0 and w_1 are the waist of the pump and injection pulse respectively. Using the experimental values, $L \simeq 1.2$ mm, which makes synchronization between the two laser pulses relatively easy.

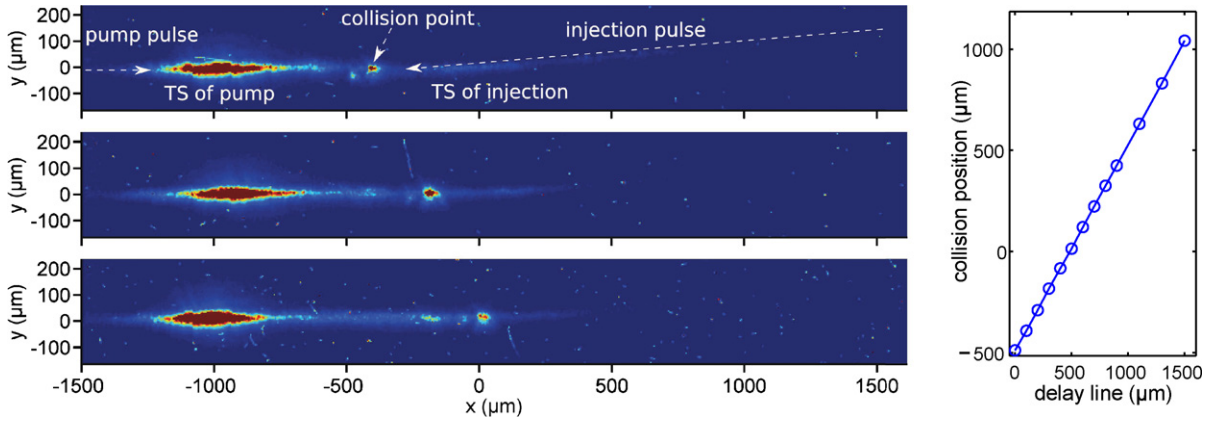

Fig. 2. Left: top view images obtained for several positions of the collision. Right: collision position versus delay line. Parameters were: $\alpha = 4°$, $a_0 = 1.5$, $a_1 = 0.4$, $n_e = 5.7 \times 10^{18}$ cm^{-3}.

For alignment at high power, a side view and a top view imaging systems were installed: each of them consisted of an achromatic lens which made an image of the plasma onto a 16 bit CCD camera. The magnification was 13 (5.8) for the side (top) view imaging. A low intensity 30 fs probe laser pulse could be sent through the side view imaging system and provided time resolved images of the plasma. This was used to synchronize the two laser pulses and to perform fine tuning of the overlapping in the vertical direction. On the top view images, Thomson scattering emission provided a way to align the beams in the horizontal plane. Note that the laser pulses were p-polarized so that Thomson scattering (TS) was more intense on the top view images than it was on the side view images (emission along the polarization direction is minimum). Finally, it was possible to insert a transmission grating (50 lines/mm) into these imaging systems in order to obtain spectral information on the scattered light.

The electron beam was measured with an electron spectrometer which gave access to the electron beam angular distribution, energy distribution and charge. The electron spectrometer consisted of a LANEX phosphor screen and a bending magnet ($B_{eff} = 1.1$ T over 10 cm). Electrons with energies greater than 45 MeV could be measured, with a resolution of 5% at 200 MeV. The charge of the electron beam was obtained by measuring the number of photons emitted by the phosphor screen. The emission of the phosphor screen was independently calibrated using a 10 MeV radio-frequency accelerator [28].

Finally, a 25 mm aperture Faraday isolator was inserted in the laser system to prevent laser feed-back from the experiment. The isolator was placed between the second (200 mJ level) and third stage amplifier (2 J level) in the laser system. Thus, the compressor gratings as well as the third stage amplifier were not protected from laser feed-back. However, no damage was observed on these optics during the first experimental campaign (for which about 3000 high power laser shots were delivered). In the second experiment, about 20 000 shots were performed over a period of 2 months and no problems ever occurred, showing that the safer non collinear geometry provides a robust and reliable operation mode.

4. Visualization of the collision using optical diagnostics

In this section, we present results obtained using optical diagnostics of the collision. Our goal is to find signatures of the injection process, such as the standing wave and/or the presence of small-scale density modulations at $\lambda_0/2$.

In the experiment, we have witnessed an enhancement of the scattered light originating from the collision. Data were collected during the second experiment ($\alpha = 4°$, 3 mm gas jet). Fig. 2 shows typical images obtained on the top view diagnostic once the two laser pulses have been overlapped and synchronized. The top image shows that the scattering from the plasma exhibits three main features: (i) TS from the pump pulse at the entrance of the density plateau (-1200 μm $< x < -800$ μm); (ii) weaker TS scattering of the injection pulse (located around $x \simeq 100$ μm); (iii) a strong signal originating from the collision region ($x \simeq -400$ μm). To prove that this scattering is linked to the collision, we have moved the collision position by changing the delay line of the injection pulse: the second and third images of Fig. 2 show that the scattering signal moves accordingly: when the delay line is moved by $2L$, the collision point moves by L (the expected value would be $L' = L\cos\alpha \simeq L$, the difference $\Delta = L - L'$ is well within the error

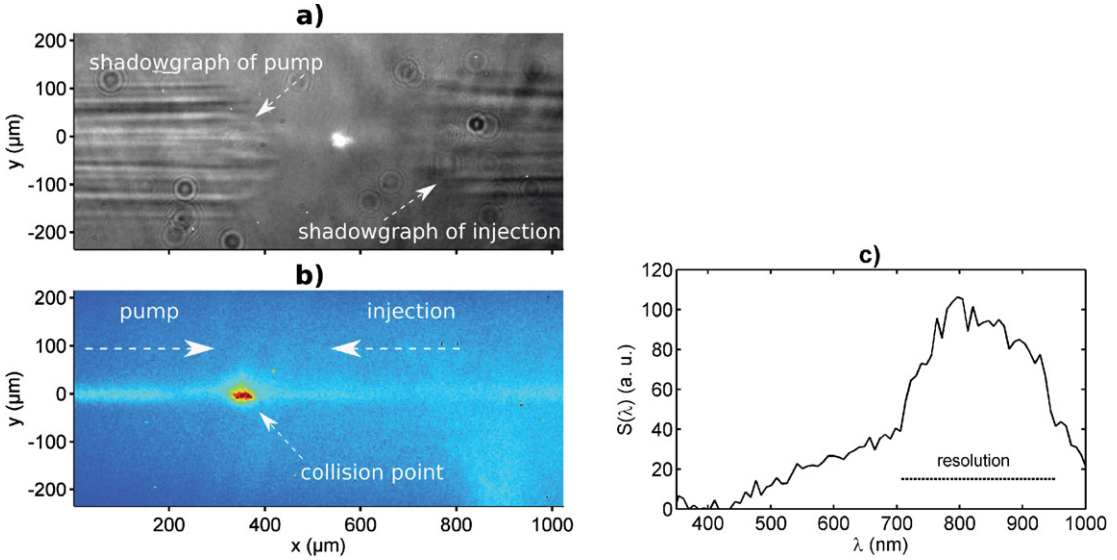

Fig. 3. Images from the side view diagnostic. a) Shadowgram obtained with the probe pulse. b) Emission from the plasma without probe pulse; parameters were: $\alpha = 4°$, 3 mm gas jet, $a_0 = 1.5$, $a_1 = 0.4$, $n_e = 5.7 \times 10^{18}$ cm^{-3}. c) Optical spectrum of the light emitted at the collision (the data was obtained with a 2 mm gas jet and $n_e = 1.5 \times 10^{19}$ cm^{-3}).

bar of the measurement). The displacement of the collision position is perfectly linear with the displacement of the delay line (which we have moved over a range of 1.5 mm, see the graph on the right of Fig. 2).

Very similar signals are obtained on the side view image. Fig. 3a) shows a shadowgraphy image taken before the collision: at this moment, the plasmas from the pump and injection pulse are separated in space. Emission from the plasma is superimposed on this shadowgram image: it shows that light is strongly emitted at a position located exactly in the middle of the two plasmas. This again suggests that this emission comes from the collision region. The emission point can also be moved by changing the delay line of the injection pulse, as above. Fig. 3b) shows the image taken without probe beam: the emission from the collision region remains. Finally, Fig. 3c) shows the spectrum of the light emitted at the collision (for plasma density $n_e = 1.5 \times 10^{19}$ cm^{-3} and a 2 mm gas jet). The spectral information was obtained by inserting a transmission diffraction grating in the imaging line. The resolution of the diagnostic is low (about 250 nm) because the beam of scattered light impinging the diffraction grating is not parallel. However, the signal clearly shows that the wavelength of emission is centered about the laser central wavelength (820 nm). Below, we summarize the behavior of this emission of light at the collision:

(i) Light originating from the collision region is collected on the side view and top view images;
(ii) This emission is usually accompanied by the generation of an electron beam (see next section);
(iii) Rotating the polarization of the injection beam causes the signal to disappear from the top view image. On the side view image, rotation of the polarization provokes a strong TS scattering signal which masks the emission from the collision so that side view imaging does not provide additional information;
(iv) The integrated signal on the top view is about 10 times stronger than it is on the side view;
(v) The wavelength is centered about 820 nm, i.e. the laser wavelength.

The first two points confirm that this emission is correlated to the physics of electron injection. The third point is highly compatible with the fact that the emission is linked to the formation of the small scale density perturbation at $\lambda_0/2$: when the polarizations are crossed, this density perturbation vanishes and there is no emission. So a natural explanation for this scattering could be that the laser pulses scatter on the small scale perturbations at the collision. The theory of Bragg scattering on small scale perturbations driven by two counter-propagating laser pulses has been studied in Ref. [29]. The authors computed the scattering of a plane wave on the density perturbations and their studies are valid within the linear approximation ($\delta n_b/n_0 \ll 1$). They showed that the density perturbations behave like a short-lived Bragg mirror which reflects the scattering wave. Although the frame of their study departs from our

experimental configuration (the linear approximation no longer holds in our experiment and the scattered waves are ultrashort), examining the results is instructive. The expected scattered spectrum is given by [29]:

$$g(\omega) = \frac{\omega_p^4}{[(\omega-\omega_s)^2-\omega_p^2]^2 + 4\gamma_L^2\omega_p^2} \times \exp\left[-(\omega-\omega_s)^2\tau^2/2\right] \tag{10}$$

where τ is the pulse duration of the colliding pulses, ω_s is the frequency of the scattering wave (for modeling our experiment, we use $\omega_s = \omega_0$) and γ_L is a factor representing the damping of small scale perturbations. For our purpose, we can take $\gamma_L = 1/\tau$, which is a way of introducing the fact that the scattering waves are the ultrashort pump and injection pulses. Using $\tau = \tau_{FWHM}/(2\sqrt{\ln 2}) = 18$ fs and $n_e = 1.5 \times 10^{19}$ cm^{-3}, one finds that the spectrum is centered at $\lambda_0 = 820$ nm, with FWHM 50 nm, in agreement with the experimental data. This behavior is almost independent on the plasma density: similar results are obtained for n_e in the 5×10^{18}–2×10^{19} cm^{-3} range.

It is also instructive to compute the angular distribution of the scattered radiation and to compare it to the experimental findings. Let us consider the following geometry: we consider the reference frame $(\mathbf{e_1}, \mathbf{e_2}, \mathbf{e_3})$ where $\mathbf{e_1}$ ($\mathbf{e_2}$) is perpendicular (parallel) to the "fringes" of the density perturbation. In this reference frame, the pump pulse propagates with wave number $\mathbf{k_0} = k_0(\mathbf{e_1}\cos(\alpha/2) + \mathbf{e_2}\sin(\alpha/2))$. The scattered wave vector is defined by $\mathbf{k_s} = k_s\mathbf{e_r}$ where $\mathbf{e_r} = \mathbf{e_1}\cos\theta + \mathbf{e_2}\sin\theta\cos\phi + \mathbf{e_3}\sin\theta\sin\phi$, θ and ϕ are angles in spherical polar co-ordinates. Assuming that the scattering laser pulses are polarized along $\mathbf{e_p}$, the scattering diagram is then given by

$$f(\theta,\phi) = [\mathbf{e_p}\times\mathbf{e_r}]^2 F^2(\theta,\phi) \tag{11}$$

where F is given by

$$F(\theta,\phi) = \exp\left[-\frac{k_0^2 w_0^2}{8} \times \left(\sin^2\theta + \sin^2(\alpha/2) - 2\sin\theta\cos\phi\sin(\alpha/2)\right) - \frac{\omega_0^2\tau^2}{4}\left(\cos\theta - \cos(\alpha/2) + 2\right)^2\right] \tag{12}$$

where w_0 is the waist of the pump pulse and τ its pulse duration. The analysis of these equations shows that the density perturbation acts like a perfect plane mirror, directing the scattered energy of the pump pulse in the direction of the injection pulse and reciprocally. In particular, Eq. (12) shows that there should not be any scattered radiation on the top view ($\theta = \pi/2$, $\phi = \pi/2$) and on the side view ($\theta = \pi/2$, $\phi = 0$). This is different from the experimental results, see (i) and (iv) above. To explain the scattering at $\theta = \pi/2$, we note that the model assumes a perfectly plane Bragg mirror and that it might not be the case in the experiment. Indeed, if the wavefronts of the laser pulses are not flat, they will give rise to density perturbations which will not be perfectly planar. Self-focusing and bubble formation could distort the wavefront of the pump laser, explaining the observed radiation.

Note that Zhang et al. [30] have observed similar radiation at the collision of two pulses (the pulses were about 10 times longer than in our experiment) and their interpretation also relied on Bragg scattering. Although they did not discuss it, they also observed radiation at 90° which is unexplained by the theory of Bragg scattering. In a recent paper, Kando et al. [31] also reported on similar emission and they suggest that this emission comes from the refraction of the injection pulse on plasma density modulations driven by the pump pulse (i.e. not related to the collision). This explanation is not satisfactory in the case of our experiment because the signal that we observed was strongly correlated to the injection pulse polarization (which should not be the case for a simple refraction phenomenon). Finally, Thomas et al. [32] have argued that electron injection can also result in broadband synchrotron emission that can be measured on top view and side view diagnostics. This is different from what we observed as the emission is not broadband in the case of our experiment. In addition, we have observed electron injection with crossed polarizations [33], even though no emission from the collision was detected.

5. Injection and acceleration of electron bunches

This emission of light at the collision is usually accompanied by the generation of an electron beam. Fig. 4 shows the characteristics of the beams that were obtained in the first experiment (collinear geometry and 2 mm gas jet). A typical electron energy distribution is shown in Fig. 4a): the beam has a quasi-monoenergetic peak at 120 MeV containing about 20 pC. For a series of 20 consecutive shots, the peak energy varies by less than 6% standard deviation (s.d.) and the energy spread $\Delta E = 12$ MeV varies by 20% s.d. The charge is the parameter which varies the most from shot to shot (about 30% s.d.) [22].

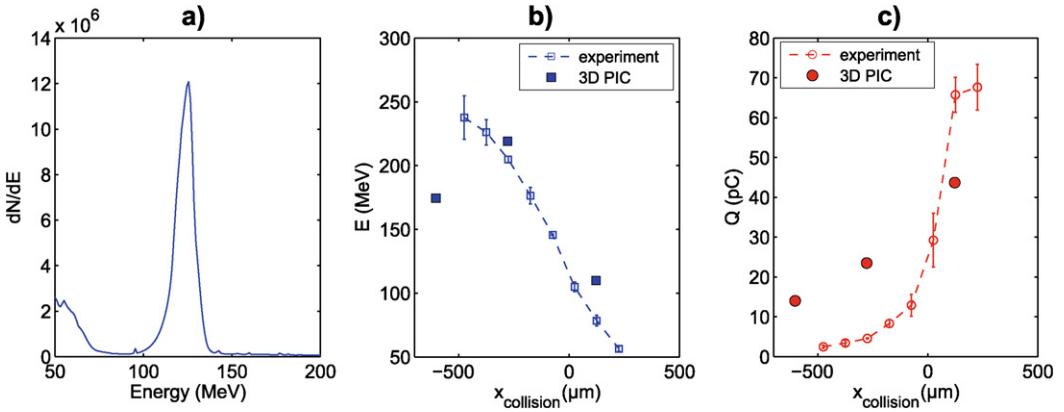

Fig. 4. Electron beam results obtained in the first experiment with a 2 mm gas jet. a) Electron energy distribution, b) electron beam peak energy as a function of collision position $x_{collision}$; empty squares: experiments, full squares: 3D PIC simulations. c) Evolution of the charge as a function of $x_{collision}$, empty circles: experiment, full circles: 3D PIC simulations. Parameters were $\alpha = 0°$, $a_0 = 1.3$, $a_1 = 0.4$, $n_e = 7.5 \times 10^{18}$ cm^{-3}. On b) and c), each point is an average of 3–5 points and the error bars represent the standard deviation.

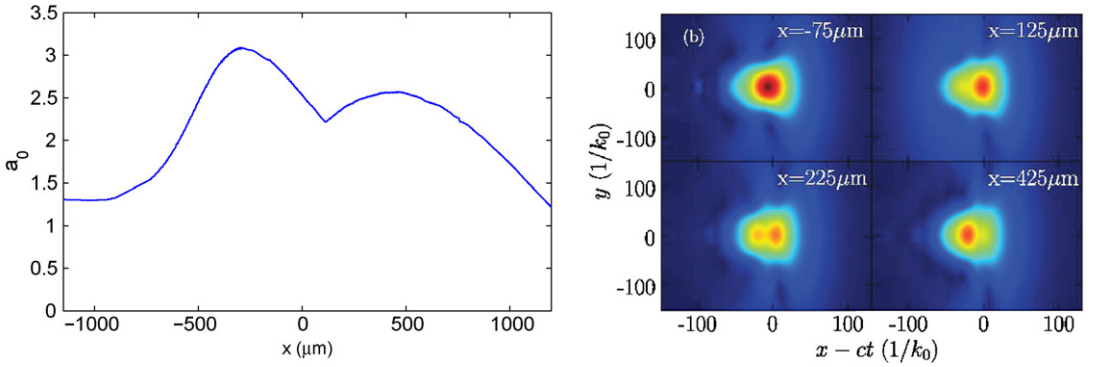

Fig. 5. Left: 3D PIC simulation of the evolution of the pump pulse normalized vector potential a_0 as a function of propagation distance (full curve). Right: spatio-temporal distortion of the laser pulse along its propagation.

In addition to enhanced stability, tuning the electron beam energy can be achieved by adjusting the collision position in the gas jet. The collision point can be modified by simply changing the delay between the two laser pulses. If the lasers collide at the entrance of the gas jet, electrons will be injected at an early stage and they can be accelerated over the whole gas jet length (2 mm). Thus, their energy will be high. On the other hand, injection at the exit of the gas jet will limit the acceleration length and will lead to a low energy beam. This is demonstrated in Fig. 4b), which shows the evolution of the beam peak energy as a function of collision position (the collision occurs at the center of the gas jet for $x_{collision} = 0$). The beam can be continuously tuned from 50 MeV to 250 MeV. The small size of the error bars illustrates the stability of the beam peak energy for all energies. In addition, one can estimate the value of the average accelerating electric field from Fig. 4b): the electron beam gains 190 MeV over 700 μm, which gives $E_z = 270$ GV/m.

Fig. 4c) illustrates the evolution of the charge in the monoenergetic peak as a function of collision position. A striking feature is that the peak charge is highest (60–80 pC) when injection occurs after the middle of the gas jet (where the peak energy is about 60 MeV) and it drops down below 10 pC when injection occurs at the entrance of the jet (for example, the charge is about 4–5 pC for a 200 MeV beam). This is of course a drawback as we would like to be able to increase the energy while keeping a large amount of accelerated charge.

3D PIC simulations have been performed in order to understand these trends in more details [34]. The simulations reproduce the experimental results quantitatively. For example, the solid squares in Fig. 4b) shows the good agreement between the peak energy obtained in the simulations and in the experiments. Fig. 4c) shows that the simulation also reproduces the trend of increasing charge as a function of collision position (solid circles), although the exact value of the charge are different from the experimental ones. Simulations show that the pulse spatial and temporal profiles

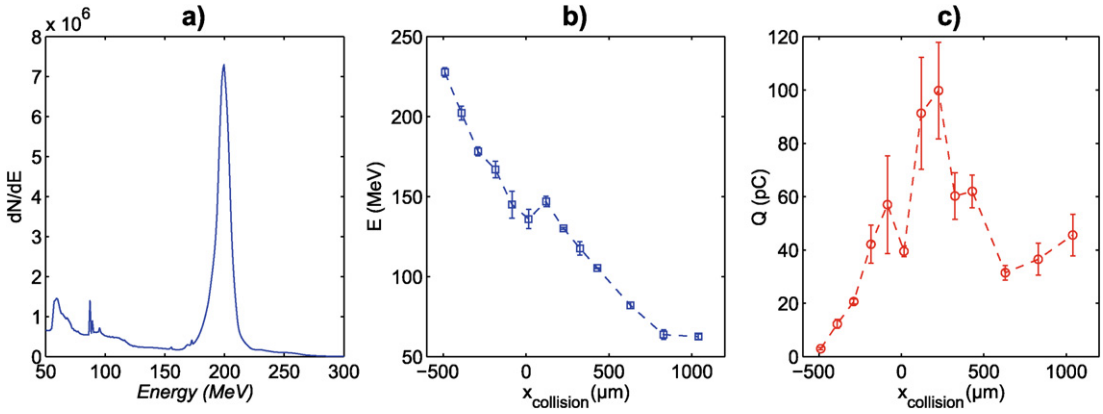

Fig. 6. Electron beam results obtained in the second experiment with a 3 mm gas jet. a) Electron energy distribution, b) electron beam peak energy as a function of collision position $x_{collision}$. c) Evolution of the charge as a function of $x_{collision}$, empty circles: experiment. Parameters were $\alpha = 4°$, $a_0 = 1.5$, $a_1 = 0.4$, $n_e = 5.7 \times 10^{18}$ cm^{-3}. On b) and c), each point is an average of 3–5 points and the error bars represent the standard deviation.

evolve through nonlinear effects (self-compression [35,36] and self-focusing) during propagation. An illustration of these phenomena is presented in Fig. 5 which shows the evolution of the pump pulse amplitude a_0 as a function of propagation (left picture). In the first half of the gas jet, the laser pulse undergoes strong self-focusing, with increasing values of a_0, up to $a_0 = 3$. Then the amplitude oscillates but the pulse stays focused. The images on the right of Fig. 5 show the laser intensity distribution for different propagation distances. The spatio-temporal modifications of the laser pulse are clearly seen; in particular, the position of the maximum intensity slips backwards as the laser propagates. This distorted laser pulse drives a distorted wakefield for which the potential is deeper over a larger radius. This enables trapping over a larger volume and could explain the larger charge. Thus, when injection occurs in the middle of the gas jet, the laser pulse is more distorted and larger amounts of electrons can be trapped. Using a longer gas jet (3 mm instead of 2 mm) should permit the injection of electrons after self-focusing has occurred, still leaving enough acceleration length for reaching 200–300 MeV energies.

Thus, in the second experiment, we have used a longer gas jet for this purpose. The results are shown in Fig. 6. An electron energy distribution at 200 MeV is presented in Fig. 6a). Note the high quality of the beam: there are very few electrons outside the peak. In addition, the beam is very stable (stability figures are similar to what has been presented above for the 120 MeV beam) and the energy spread ($\Delta E = 14$ MeV) is limited by the resolution of the spectrometer. Note that the beam charge at 200 MeV is about 13 pC, i.e. three times higher than in the first experiment. Figs. 6b) and 6c) show the evolution of energy and charge of the beam. The tuning of the energy from 60 to 240 MeV is still possible even though the laser pulses propagate at a small angle because the overlap region is still about 1 mm. The charge evolution can be seen as the superposition of a peak around $x_{collision} = 200$ μm giving beam charges as high as 100 pC, and a linear increase of charge with the collision position. The peak can be explained by the use of the non collinear geometry: there is an optimal position for which the two beams overlap, thus explaining the charge maximum. The monotonic increase of charge, from 3 pC at the early injection position ($x_{collision} = -500$ μm) to 50 pC for late injection position ($x_{collision} = 1000$ μm), is due to the nonlinear pulse evolution as we have seen earlier.

Fig. 7 presents a comparison of the charge as a function of energy for the two different gas jet lengths. It is clear that the use of a longer gas jet produces larger injected charge for energies in the 100–200 MeV range. Thus, by increasing the interaction length before performing injection, we have been able to optimize the charge at high energy.

6. Conclusion

The injection of electrons into plasma waves using two counter-propagating laser pulses has been demonstrated experimentally during two campaigns and over long periods of time. It is a robust, reproducible scheme which is very promising for the future of laser–plasma accelerators. The physics at stake is now well understood and PIC simulations reproduce the experimental results with quantitative agreement. We have seen that the understanding of pump pulse propagation has led us to using longer gas jets, leading to an increase of the beam charge at high energy. However, there is still room for improvement: reaching energies in the GeV range with higher charge would be desirable, especially

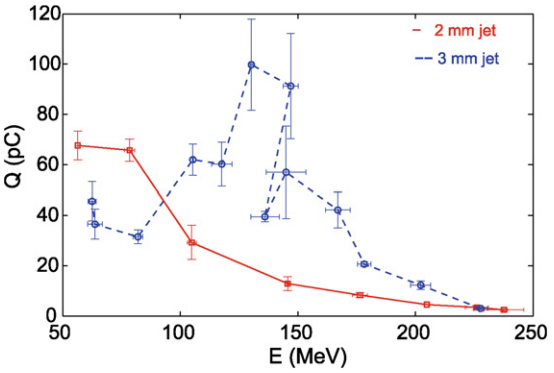

Fig. 7. Charge in the quasi-monoenergetic peak as a function of energy for the 2 mm nozzle (squares, dashed line) and the 3 mm nozzle (circles, full line).

for demanding applications such as the generation of X-ray radiation in a free electron laser. Obviously, the key issue will be to perform these improvements while maintaining the best beam quality: emittance, bunch duration and energy spread should be kept as low as possible.

Acknowledgements

This work has been partially supported by ANR-05-NT05-2-41699, by the European Community Research Infrastructure Activity under the FP6 Structuring the European Research Area program (CARE, contract number RII3-CT-2003-506395 and EUROLEAP, contract number 028514) and by the RTRA Triangle de la Physique (APPEAL project).

References

[1] T. Tajima, J.M. Dawson, Laser electron accelerator, Phys. Rev. Lett. 43 (4) (1979) 267.
[2] S.V. Bulanov, et al., Transverse-wake wave breaking, Phys. Rev. Lett. 78 (22) (1997) 4205–4208.
[3] A. Pukhov, J. Meyer-ter-Vehn, Laser wake field acceleration: the highly non-linear broken-wave regime, Appl. Phys. B 74 (2002) 355–361.
[4] W. Lu, et al., Nonlinear theory for relativistic plasma wakefields in the blowout regime, Phys. Rev. Lett. 96 (2006) 165002. [Online]. Available: http://link.aps.org/abstract/PRL/v96/e165002.
[5] S.P.D. Mangles, et al., Monoenergetic beams of relativistic electrons from intense laser–plasma interactions, Nature 431 (2004) 535–538.
[6] C.G.R. Geddes, et al., High quality electron beams from a laser wakefield accelerator using plasma-channel guiding, Nature 431 (2004) 538–541.
[7] J. Faure, et al., A laser–plasma accelerator producing monoenergetic electron beams, Nature 431 (2004) 541–544.
[8] W.P. Leemans, et al., GeV electron beams from a centimeter-scale accelerator, Nat. Phys. 2 (2006) 696–699.
[9] J. Osterhoff, et al., Generation of stable, low-divergence electron beams by laser-wakefield acceleration in a steady-state-flow gas cell, Phys. Rev. Lett. 101 (8) (2008). [Online]. Available: http://dx.doi.org/10.1103/PhysRevLett.101.085002.
[10] S.P.D. Mangles, et al., On the stability of laser wakefield electron accelerators in the monoenergetic regime, Phys. Plasmas 14 (5) (May 2007) 056702.
[11] N.A.M. Hafz, et al., Stable generation of GeV-class electron beams from self-guided laser–plasma channels, Nat. Photonics 2 (Sep. 2008).
[12] M. Everett, et al., Trapped electron acceleration by a laser-driven relativistic plasma wave, Nature 368 (1994) 527–529.
[13] F. Amiranoff, et al., Observation of laser wakefield acceleration of electrons, Phys. Rev. Lett. 81 (1998) 995.
[14] S. Bulanov, et al., Particle injection into the wave acceleration phase due to nonlinear wake wave breaking, Phys. Rev. E 58 (5) (Nov. 1998) R5257–R5260.
[15] C.G.R. Geddes, et al., Plasma-density-gradient injection of low absolute-momentum-spread electron bunches, Phys. Rev. Lett. 100 (2008) 215004.
[16] C.I. Moore, et al., A laser-accelerator injector based on laser ionization and ponderomotive acceleration of electrons, Phys. Rev. Lett. 82 (8) (Feb. 1999) 1688–1691.
[17] D. Umstadter, J.-K. Kim, E. Dodd, Laser injection of ultrashort electron pulses into wakefield plasma waves, Phys. Rev. Lett. 76 (1996) 2073.
[18] E. Esarey, et al., Electron injection into plasma wake fields by colliding laser pulses, Phys. Rev. Lett. 79 (1997) 2682.
[19] R.G. Hemker, et al., Computer simulations of cathodeless, high-brightness electron-beam production by multiple laser beams in plasmas, Phys. Rev. E 57 (5) (May 1998) 5920–5928.
[20] G. Fubiani, et al., Beatwave injection of electrons into plasma waves using two interfering laser pulses, Phys. Rev. E 70 (2004) 016402.

[21] H. Kotaki, et al., Head-on injection of a high quality electron beam by the interaction of two laser pulses, Rev. Sci. Instrum. 72 (2004) 2961–2965.
[22] J. Faure, et al., Controlled injection and acceleration of electrons in plasma wakefields by colliding laser pulses, Nature 444 (2006) 737–739.
[23] J. Faure, et al., Controlled electron injection in a laser–plasma accelerator, Plasma Phys. Controlled Fusion 49 (2007) B395–B402.
[24] J.T. Mendonça, Threshold for electron heating by two electromagnetic waves, Phys. Rev. A 28 (6) (1983) 3592–3598.
[25] Z.-M. Sheng, et al., Stochastic heating and acceleration of electrons in colliding laser fields in plasma, Phys. Rev. Lett. 88 (5) (2002) 055004.
[26] A. Bourdier, D. Patin, E. Lefebvre, Stochastic heating in ultra high intensity laser–plasma interaction, Physica D Nonlinear Phenomena 206 (2005) 1–31.
[27] G. Fubiani, Controlled electron injection into plasma accelerators and space charge estimates, Thèse de doctorat, Université Paris XI Orsay, 2005.
[28] Y. Glinec, et al., Absolute calibration for a broad range single shot electron spectrometer, Rev. Sci. Instrum. 77 (2006) 103301.
[29] L. Gorbunov, A. Frolov, Collision of two short laser pulses in plasma and the generation of short lived Bragg mirrors, Sov. Phys. JETP 93 (2001) 510–518.
[30] P. Zhang, et al., An optical trap for relativistic plasma, Phys. Plasmas 10 (2003) 2093.
[31] M. Kando, et al., Demonstration of laser-frequency upshift by electron-density modulations in a plasma wakefield, Phys. Rev. Lett. 99 (13) (2007) 135001. [Online]. Available: http://link.aps.org/abstract/PRL/v99/e135001.
[32] A.G.R. Thomas, et al., Measurements of wave-breaking radiation from a laser-wakefield accelerator, Phys. Rev. Lett. 98 (5) (2007) 054802. [Online]. Available: http://link.aps.org/abstract/PRL/v98/e054802.
[33] C. Rechatin, et al., Quasimonoenergetic electron beams produced by colliding cross-polarized laser pulses in underdense plasmas, New J. Phys. 11 (2009) 013011.
[34] X. Davoine, et al., Simulation of quasimonoenergetic electron beams produced by colliding pulse wakefield acceleration, Phys. Plasmas 15 (2008) 113102.
[35] F.S. Tsung, et al., Generation of ultra-intense single-cycle laser pulses by using photon deceleration, Proc. Nat. Acad. Sci. 99 (1) (2002) 29–32.
[36] J. Faure, et al., Observation of laser pulse shortening in nonlinear plasma waves, Phys. Rev. Lett. 95 (2005) 205003.